Optical and Infrared Imaging of Growing Polyolefin Particles

Jochem T. M. Pater, Günter Weickert and Wim P. M. van Swaaij
Process Technology Institute Twente, University of Twente, High Pressure Laboratories, NL-7500AE Enschede, The Netherlands

A method was developed that observes polymer particles during a polymerization reaction using optical- and infrared imaging. The yielding images give good insight into catalyst-specific properties as shape replication, distribution of activity, and the activation. The advantage of this method is the possibility to link behavior of individual particles to its own specific properties. The infrared method measures surface temperatures of growing particles. Such data are useful to feed mathematical models describing the growth of single particles. The temperature–time curves showed maximum temperature to be reached after some minutes; a simple model was used to describe this effect qualitatively. The maximum particle temperature rise was 20 K, but depended strongly on reaction rate and particle size. Temperature, prepolymerization method, catalyst recipe, and catalyst activation time were varied for a fourth-generation Ziegler-Natta catalyst in polymerization of propylene and ethylene.

Introduction

There has been a huge expansion of polyolefins into worldwide plastics markets over the past decades. The world market share of polyolefins was around 20% of the total thermoplastic market in the 1960s. Today, polypropylene and polyethylene account for almost 60% of the global plastic production with an annual increase of 7–8% (Galli, 1995). Developments in new catalysts are combined with developments in new process technologies, which lead to new products with new properties. The success of these materials is a result of the combination between the excellent cost-performance balance and the environmentally friendly aspects of the processes used to make them, as well as of the products. The advances in the catalyst materials and process technologies are the result of continued strong efforts in research and development, and in improving the understanding in the involved mechanisms.

However, a characteristic of these investigations is the averaging of properties over a large number of particles. When looking into kinetics and/or morphology development of the growing particles, it is common to use batch experiments where an amount of catalyst material is introduced into a polymerization reactor. After the polymerization run, the product is evacuated from this reactor and analyzed on polymer properties—using methods like DSC, GPC, and MFR—and on powder properties by using methods like electron microscopy, particle-size analysis, and porosity measurements. Average properties of the catalyst material, like metal concentrations and particle sizes, are related to average properties of the product, combined with the overall measured reactor conditions.

In addition, properties of the particles are, as already mentioned, measured after removing the product from the polymerization system. It is well known that evacuation of the product from the reactor, involving huge changes in pressure and temperature, can change some properties of the product, such as crystallinity, even before these properties are determined.

These two disadvantages would be overcome if individual particles were observed during the polymerization process. A

Correspondence concerning this article should be addressed to G. Weickert.

polymerization cell with online and *in-situ* analysis and characterization methods would solve these difficulties. In this work, we will present a microreactor composed of such a cell with a transparent lid. It comes in two different configurations:

- In the first system, an optical camera is connected to the setup and optical images are obtained from the growing polypropylene particles. This application is used to study shape development of the particles and reaction kinetics.
- In the second application, the system is used for infrared observation of the growing particles. In this way, surface temperatures of the particles can be obtained *in situ*, without disturbing the particles. This application will be of importance in supporting single particle modeling efforts.

Optical imaging in olefin polymerization reactions

Different groups have shown such applications, related to these polymerizations, in literature before. The use of electron microscopy in combination with growing particles in catalyzed olefin polymerization was shown in the 1970s for the first time (Baker et al., 1973) and was repeated after that by others (Corradini et al., 1988).

In 1996 the Reichert group showed the application of the optical observation of growing polybutadiene particles at low pressures (Eberstein et al., 1996). After that, the method was further improved by Bartke and Zoellner (Zoellner and Reichert, 2001; Bartke et al., 2003).

More recently, other groups have also described their work using similar techniques (Kaneko, 2000; Oleshko et al., 2001). Since 1998, our group has been performing investigations using a reaction cell with transparent lid, to study the catalytic polymerization of propylene (Weickert et al., 1999; Pater et al., 2001) at elevated pressures, up to 35 bars, so at industrially relevant conditions.

Infrared imaging in chemical engineering

The idea of infrared imaging is used in different applications, both within and outside chemical engineering. This powerful tool in studies to surface temperatures is known in catalysis research. Investigation of temperature profiles on the surface of catalytic active materials in different systems shows the power of the method. The applicability of IR thermography in heterogeneous catalysis was demonstrated already in 1987 (Pawlicki and Schmitz, 1987). The Luss group published a number of articles on the use of IR thermography in different systems to study temperature profiles on the surfaces of catalytic materials (Annamalai et al., 1997, 1999; Liauw et al., 1997; Lobban et al., 1989; Moates et al., 1996; Somani et al., 1997). The same idea was used in the development of a catalyst screening method in the Reetz group (Reetz et al., 2000, 1998a,b; Holzwarth et al., 1998). In that work, IR thermographic detection was used to identify catalytic activity in libraries of heterogeneous catalysts. The use of IR thermography as a screening method in a combinatorial way allows testing of large numbers of complexes in terms of activity and selectivity. The use of IR thermography in catalytic olefin polymerization was not reported before, as the demands in this area were up to now incompatible with the technical possibilities. The particle sizes of the catalyst particles are between 15 and 100 micron, requiring relatively strong magnification possibilities on the infrared camera system. Despite the fact that efforts have been made for decades to calculate particle temperatures during polymerization, it was never possible to measure the real temperatures. Measuring bulk temperatures will not provide the particle temperatures, and the use of direct contact in particle measurements would lead to disturbance of the particle's heat balance. Application of a contact-less method to determine the particle temperature is, therefore, obvious. Previous mentioned articles demonstrate the benefits of infrared thermography in this relation.

Objective

The aim of this work is to show the possibilities of direct observation methods in a system operating at industrially relevant conditions, respecting the circumstances needed in catalytic olefin polymerization: high purity of the polymerization cell, highly purified starting chemicals, and a reproducible procedure in catalyst preparation. Also, the applicability of this method for catalyst screening and for kinetic measurements will be tested.

The experimental equipment and procedures are described. The results of the optical observation of catalytic polymerization reactions are then shown, followed by discussion of those results. Subsequently, the results of the infrared observation of the reacting system are presented. With the discussion of the temperature measurements, a simple model of mass- and heat-balances is used to qualitatively describe the particle temperatures during polymerization. Although only a restricted number of experiments are shown here, the results are indicative for the results observed in a large number of experimental tests.

Experimental Studies

Chemicals

The catalyst used in this work is a commercially available Ziegler-Natta catalyst of the fourth generation, with $TiCl_4$ on a $MgCl_2$ support. As cocatalyst, triethyl aluminum was applied, kindly donated by AkzoNobel. As an external electron donor, dicyclo pentyl dimethoxy silane (the so-called D-donor) was taken. To suspend the catalyst, hexane of "Pro Analysi" quality obtained from Merck was used. The propylene used was obtained from Indugas, with a purity $>99.5\%$, and with propane as main impurity. The hydrogen and nitrogen used were of $>99.999\%$ purity.

The hydrogen, nitrogen, and hexane were extra purified by passing them over a reduced BTS copper catalyst, and subsequent passing them over three different molecular sieve beds, with pore sizes of 13, 4 and 3 angstrom, respectively. The BTS catalyst was obtained from BASF. The propylene was purified in the same way, after it was passed over a bed of oxidized BTS copper catalyst.

Equipment

The microreactor setup used here consists basically of two parts (Figure 1). The first part (A) is the polymerization cell in which the polymerization reactions are carried out. The second part (B + C) is the connected observation system with

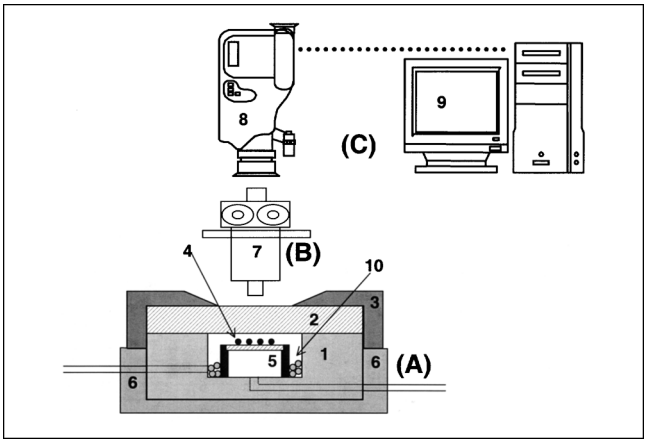

Figure 1. Microreactor setup, with (1) the body of the cell, (2) the transparent lid, (3) the metal lock for the lid, (4) catalyst, (5) support material for particles and (6) heating jacket.

In the observations, (7) a microscope is used combined with (8) the observation system. This camera is connected to (9) the PC for data acquisition. Polymer particles treated with (10) TEA are used for scavenging.

which information is collected on the growing polymer particles.

Polymerization Cell. The polymerization reaction is carried out in a polymerization cell. The 6-mL stainless steel cell (1) has a transparent lid (2) to allow particle observation. The lid is mounted tightly with a metal ring (3) to permit pressures up to 40 bar without leaking. Catalyst particles (4) are distributed on the support disk (5). The polymerization cell is placed in a thermostatic jacket (6) to ensure a constant temperature in the cell over time.

The cell has two inlets. The first inlet is used for the evacuation of the cell and for introducing process gas in tangential direction. The second can be used as a gas outlet, or for the introduction of thermocouples. The tip of the thermocouple is located in the gas phase underneath the glass support disk.

Optical Observation. When the system is used for optical observation of the growing polymer particles, a *Pieper FK 7512-IQ* digital camera is connected to the *Carl Zeiss Axiotech Vario 25 HD* microscope ((B) in Figure 1). The microscope is equipped with different objectives, providing different features. Table 1 shows an overview of the different objectives used in the system. Next to the internal light source of the microscope, a second, external light source is used to obtain good contrast of the polymer particles on their background. The digital camera is connected to a frame grabbing PC with imaging software. With a preset frequency, images of the polymer particles are saved.

Infrared Observation. When the system is used for infrared observation, a *ThermaCAM PM 290* camera of Inframetrics is used with an *Inframetrics* microscope objective. This camera observes the infrared emission from the polymerization cell and determines the intensity of the radiation with a wavelength between 3.4 and 5.0 μm with an update rate of 50 Hz. The camera uses a 256×256 platinum silicide focal plane array detector. An integrated closed-cycle cryogenic cooler maintains the low detector temperature of 77 K. Using the mentioned microscope objective, one pixel in the image equals 6.3×6.0 μm.

Procedures

Preparation of the Catalyst. The catalyst, suspended in a mineral oil, is weighed out in the glovebox under a nitrogen atmosphere and, subsequently, hexane, a 4 mg/g TEA solution in hexane, and a 2 mg/g donor solution in hexane are added to the catalyst to activate it. The suspension is gently shaken for 15 min at room temperature, and the liquid is then removed from the catalyst after settling the solids. To be able to reproduce the amount of TEA remaining at the catalyst, the catalyst is washed with fresh hexane once, and, after removal of the washing fluid, it is dried at room temperature in a vacuum. In this way, an activated, dry, free flowing catalyst powder is obtained.

The dry catalyst is dispersed on the background material, which is, in this case, a 25-mm diameter plate of a dark colored glass, in such a way that the observable area of the optical microscope will contain about 10 catalyst particles. Careful tapping with the support glass will distribute the catalyst on the surface. A small amount of polyethylene powder is placed around the metal ring in the polymerization cell that was treated with a triethyl aluminum alkyl solution in hexane (indicated with (10) in Figure 1). The polymer powder with active aluminum will scavenge impurities from the incoming gas, however, due to the low vapor pressure of the alkyl, it will not show cocatalytic activity. The reaction cell is then closed in the glovebox and brought to reaction conditions at the setup.

Polymerization Procedure. The cell is placed in the heated jacket to be brought to the reaction temperature. Introducing the preheated and premixed process gas into the reactor starts the polymerization reaction. Typically, this process gas will be the mixture of different monomers, which, in the present work, are ethylene and propylene. Hydrogen is a chain transfer agent and nitrogen is an inert gas. Just before the introduction of the process gas, the observation system—infrared or optical—is started. Normally, the reaction is continued for 20 min; releasing the pressure will stop the reaction.

When applying one or two prepolymerization steps in the experiment, the reactor is set to prepolymerization tempera-

Table 1. Properties of the Three Objectives used in the Microscope of the Optical Microreactor System

Type	Magnification	Numerical Aperture	Resolution of Lens (μm)	Resolution of Camera (μm)	Depth of Field (μm)	Working Distance (mm)	Observable Area (mm$\times$mm)	Spherical Aberration (μm)
Epiplan 4x/0.10	4	0.1	3.3	4.1	55	19.8	2.1×2.1	0.4
Epiplan 10x/0.25	10	0.25	1.3	1.3	9	12.6	0.8×0.8	6.0
Epiplan 20x/0.40	20	0.4	0.8	0.8	3	9.8	0.4×0.4	29

ture, which is typically 40°C. The process gas is introduced, and, after the prepolymerization time (typically 2 min), the system is evacuated. When two prepolymerization steps are used, this is repeated with another gas composition or at another polymerization temperature. After prepolymerization steps, the reactor is brought to the conditions of the main polymerization, typically 70°C, and the process gas is introduced after reaching that temperature. No monomer is, therefore, present during changing the temperature of the cell, and, thus, no reaction can take place.

Determination of single particle polymerization rates

When the optical observations are used, a two-dimensional (2-D) image of the growing polymer particles is obtained. With a preset interval, here every 10 s, the optical image of the growing polymer particles is stored on the hard disk. After the experiment, imaging software is used to determine the size of the 2-D representation of all the present catalyst/polymer particles in every picture. This is an important step in the data processing. Due to spherical aberration, blooming and background blurring, the boundary of the particle is often not easy to recognize. In every picture, an "intensity threshold" has to be determined that indicates if a pixel belongs to the particle or to the background. Figure 2 illustrates these effects. Figure 2a shows a polymer particle without a reactor lid, and, in Figure 2b, the same particle is shown through an 8-mm glass window. The lid spreads the light from the particle, mainly due to spherical aberration of the glass. With increasing magnification of the microscope objective, the spherical aberration will increase, or by reducing the thickness of the lid, this effect can be minimized. For example, the last column of Table 1 shows the measure of spherical aberration when using an 8-mm thick borate glass lid. By using a sapphire window, the thickness can be reduced without affecting the maximum allowable pressure in the cell. Here a 2-mm thick sapphire window was used, allowing maximum pressures of 27 bar.

After determination of the mentioned threshold, the 2-D surface area can be calculated into a 3-D particle volume. An important assumption is made here that the particles do have a spherical shape. The increase of the particle volume is then transformed into a polymerization reaction rate, using the density and porosity of the polymer.

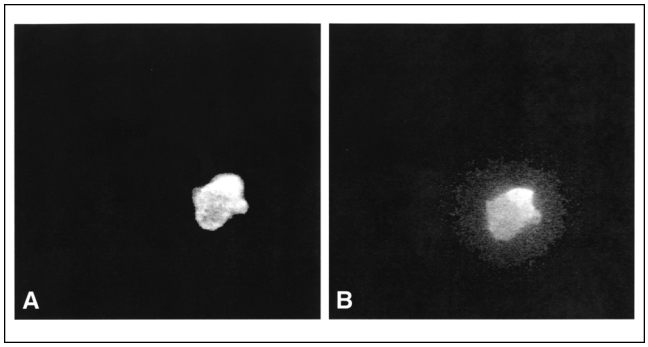

Figure 2. Effect of spherical aberration.

(A) image taken without transparent lid; (B) image taken with the 8-mm thick lid, causing dispersion of the light.

Results: Optical Observations

Reproducibility

Due to the fact that the amount of catalyst used is small and the surface of the reactor wall is relatively large, impurities will be an important issue in this system. Figure 3 shows a typical representation of the growth rate of different particles during the same polymerization experiment vs. time, extracted from the 2-D images, by using the method described before. The scattering that is shown in this figure is due to the poor contrast at the boundary of the polymer particle. As mentioned earlier, the lid of the cell causes spherical aberration. Therefore, the edges of the polymer particles are not sharp on the black background, but rather show a fading contrast, and it is, therefore, hard to determine the exact edge of

Table 2. Recipes used in the Experiments of This Work

	Catalyst Activation							Main Polymerization						
Exp.	Catalyst (μmol)	TEA (μmol)	Donor (μmol)	T_{act} (°C)	t_{act} (min)	V_{act} (mL)	Prepol*	T_{reac} (° C)	$C_3^=$ (bar)	$C_2^=$ (bar)	H_2 (bar)	N_2 (bar)	*Rp* (kg/g·h)	Bandwidth (kg/g·h)
1	6.5	260	130	20	15	10.7	none	40	8.7	–	0.5	1.1	0.27	0.22–0.33
2	6.5	260	130	20	15	10.7	none	50	9.1	–	0.5	1.1	0.35	0.29–0.40
3	6.5	260	130	20	15	10.7	none	60	9.3	–	0.5	1.1	0.47	0.41–0.53
4	6.5	260	130	20	15	10.7	none	70	9.3	–	0.5	1.1	0.72	0.60–0.85
5	6.5	260	130	20	1,080	10.7	none	50	9.4	–	0.5	1.1	0.35	0.30–0.40
6	6.5	260	130	20	1	10.7	none	50	9.2	–	0.5	1.1	0.37	0.34–0.43
7	6.5	2,600	1,300	20	15	10.7	none	50	9.5	–	0.5	1.1	0.38	0.34–0.43
8	6.5	26	13	20	15	10.7	none	50	9.4	–	0.5	1.1	0.36	0.32–0.41
9	6.5	2,600	1,300	20	1,080	10.7	none	50	9.1	–	0.5	1.1	0.35	0.29–0.40
10	6.5	26	13	20	1	10.7	none	50	9.3	–	0.5	1.1	0.37	0.33–0.42
11	6.5	260	130	20	15	10.7	method 1	70	9.4	–	0.5	1.1	0.70	0.59–0.81
12	6.5	260	130	20	15	10.7	method 2	50	9.0	–	0.5	1.1	0.85	0.70–1.00
13	6.5	260	130	20	15	10.7	method 3	40	8.9	–	0.5	1.1	0.26	0.20–0.30
14	6.5	260	130	20	15	10.7	method 1	40	8.4	1.0	0.5	1.1	0.43†	0.40–0.48
15	6.5	260	130	20	15	10.7	none	50	8.0	1.0	0.5	1.1	1.20	1.00–1.40
16	6.5	260	130	20	15	10.7	none	67	15.0	–	0.5	0.0	1.15	0.98–1.30

*Prepolymerization methods are described in Table 4.
†Reaction increased in 4 min to a final value of 0.43.

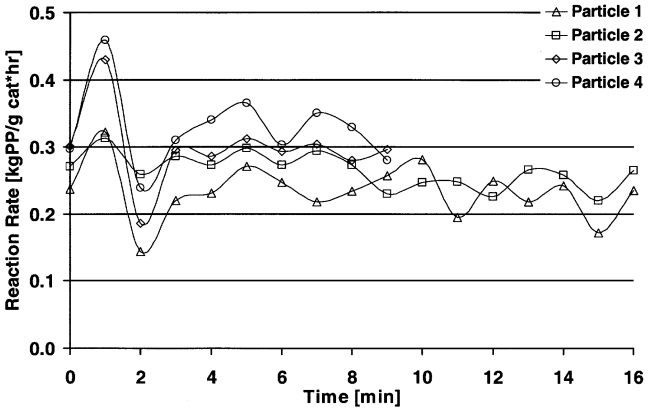

Figure 3. Reaction rate in time for four different particles in the same polymerization experiment: homopolymerization of propylene at 70°C.

the particle. During determination of the surface of the 2-D projection of the particle, pixels belonging to the background can be counted "in" or particle pixels can be left out, resulting in a scattering reaction rate in time. The last column in Table 2 shows the bandwidth of the activities of different experiments at the same conditions.

It is seen that different particles in the same experiment show very similar behavior: they start growing at the same time and at the same reaction rate with respect to their initial volume. However, in a comparison between different experiments, reproducibility is poorer. It is hard to make a direct comparison, as reaction rates are scattering due to spherical aberration and background blurring. By increasing the number of experiments, there is no problem to draw solid conclusions from experimental results.

Shape replication and induction period

As stated before, shape development and the morphology of the product are important issues in modern polyolefin technologies. With the present method, it is possible to observe a large number of different particles in the same experiment. In Figure 4, images are shown of growing polymer particles at different moments during a copolymerization experiment. From Figure 4, it can been seen that the shape of the particles does not change with time. The shape of the catalyst particles is globally replicated, and is invariant during the reaction.

It also seems as if all particles start growing at the same moment. In movies constructed from the pictures one sees that in the first few images, passing only 10 s, all the particles start already growing.

With imaging software, the pictures, similar to ones in Figure 4, can be interpreted. Figure 5 shows the relation between the initial particle size of the catalyst particle and its reaction rate in propylene polymerization. It is clear that when reaction rate is expressed per amount of catalyst, reaction rates do not depend on this initial particle size. The dotted lines in the figure indicate the bandwidth of the values of the activity. This band is the same as indicated in the last column of Table 2.

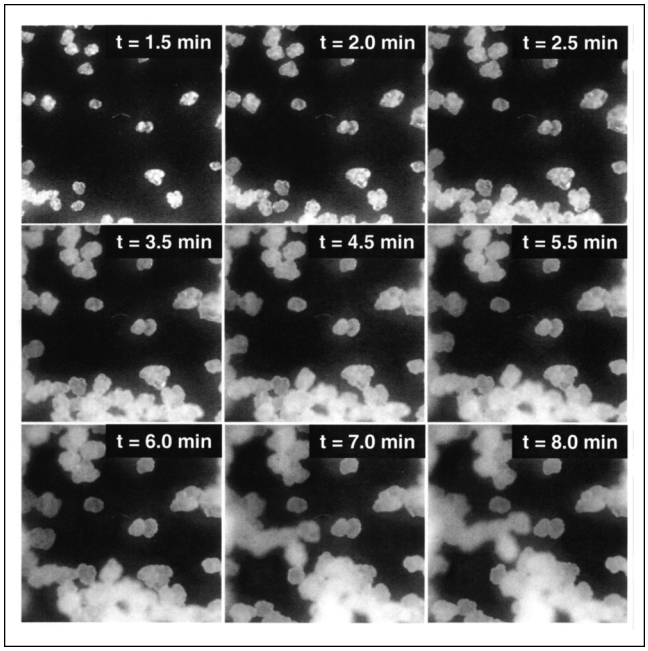

Figure 4. Replication of shape in copolymerization experiment (experiment 15 in Table 2).

Images are taken after 1.5, 2.0, 2.5, 3.5, 4.5, 5.5, 6.0, 7.0 and 8.0 min. The width of an image represents a length of 850 micron in reality.

Influence of catalyst preparation

The influence of the duration of activation and of the concentrations of cocatalyst and electron donor during activation was tested in several series of experiments. In the first series, normal activation concentrations of D-donor and TEA were used, but activation time was varied strongly: 1 min, 15 min, and 1,080 min. Table 2 shows that the single particle reaction rates calculated from these experiments were not influenced by this changing activation time.

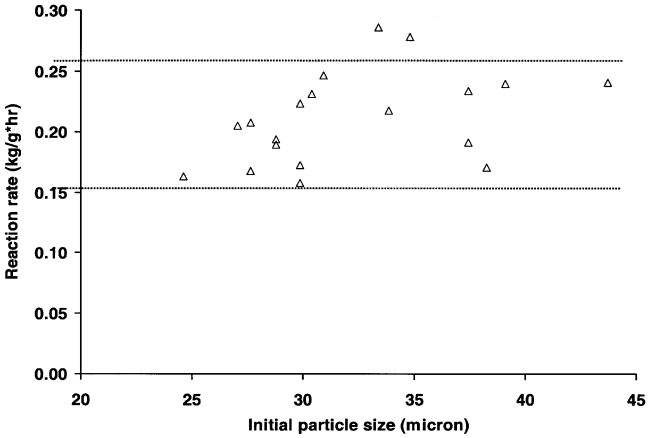

Figure 5. Relation between initial size of catalyst particles and reaction rate in gas-phase polymerization in microreactor, calculated from optical observation for 19 particles.

In experiments where concentrations of D-donor and cocatalyst were varied strongly at constant activation times, the same constant reaction rates were observed. While maintaining a constant Al/Si mole ratio of 2, the Si/Ti mole ratio in the activation fluid was varied from 2, 20, and 200. In all these tests, no influence was seen on reaction rates.

To combine the most extreme cases with each other, the catalyst was activated for 1,080 min at Si/Ti mole ratio of 200 and for 1 min at Si/Ti mole ratio of 2. Even in these cases, reaction rate was at the same value, as can be seen in Table 2.

Influence of temperature

The present method can be used to determine the kinetics of the individual particles. A series of experiments were carried out at different polymerization temperatures. In these tests, standard conditions were used as shown in Table 2. The polymerization temperature was varied from 40 to 70°C. The resulting reaction rates are listed in the same table as experiments 1 to 4. When taking into account the spread in activity of the different particles in the same experiment, one can determine from this plot an activation energy for the temperature dependence of the rate according to Arrhenius. Figure 6 shows the kinetics results from those tests indicated with the triangle-shaped markers, plotted as natural logarithm of the reaction rate vs. the reciprocal temperature. It is obvious that reaction rates increase with increasing temperature and this relation seems to be linear. Activation energy determined in this plot is around 52 kJ/mole.

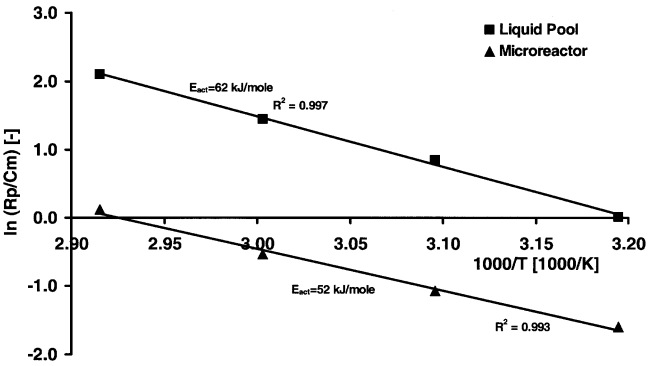

Figure 6. Temperature dependency of reaction rate in: gas-phase polymerization (microreactor) vs. liquid pool polymerization (propylene polymerization in liquid monomer).

This takes into account the difference in monomer concentration at the active sites.

Pre- and copolymerization

The influence of temperature on polymerization kinetics is shown above. When one would like to compare this influence for the gas-phase polymerization, with, for example, kinetics in liquid pool polymerization of propylene (being the bulk polymerization in liquid monomer), as will be discussed in the next section, one has to keep in mind the experimental differences. One of the differences in these two cases is the heat removal from the polymerizing particles. If reaction rates would be high in the initial stage of the gas-phase polymerization, one could expect thermal runaway on particle scale due to too low heat removal capacity of the gas phase. A method to overcome this problem would be the use of a prepolymerization step. In this prepolymerization, the system is started up at a low polymerization temperature for a few minutes. The system is then evacuated to stop the polymerization, the cell is brought to the reaction temperature, and the reaction is started up again. By doing this, the outer surface area of the particles would be enlarged by the prepolymerization, possibly avoiding runaway during the main polymerization. It is widely accepted in literature that, in these polymerization reactions, the heat-transfer resistance is at the boundary between the particle and the gas phase. Temperature profiles inside the polymer particle can be neglected.

Experiment 11 in Table 2 shows that activity in experiments including a prepolymerization step does not differ from activity in experiments without this prepolymerization step (for example, experiment 4 in the same table). From that, one can conclude that this thermal runaway does not reduce activity in a "normal" experiment. In the second part of this work, we will go into more detail with respect to particle temperatures during polymerization, by using the infrared observation system.

Because of the size of the polymerization cell, the system can be run very flexibly. A series of experiments were run using different prepolymerization procedures, including prepolymerization steps in the presence of ethylene. The accelerating effect of the presence of ethylene on the polymerization of propylene is well known in these systems, but this effect is still not fully understood. Table 3 shows different prepolymerization methods that were used in these experiments. In the second and the third method, the catalyst was prepolymerized in different variations, in the presence of ethylene as comonomer. Experiments 11 to 13 in Table 2 show the influence of these prepolymerizations on the reaction rate in the main polymerization with propylene. When defining the reaction rate in propylene main polymerization at 70°C as "normal," one can see that the reaction rate in this main polymerization reaches doubled activity when ethylene was present during the prepolymerization step. Even when the system is evacuated after the prepolymerization step and the presence of "free" ethylene is unlikely, reaction rate in the

Table 3. Methods used for Catalyst Prepolymerization by Changing Gas Composition

	1st Prepolymerization						2nd Prepolymerization					
Prepol Method	T_{prepol} (°C)	t_{prepol} (min)	$C_2^=$ (bar)	$C_3^=$ (bar)	H_2 (bar)	N_2 (bar)	T_{prepol} (°C)	t_{prepol} (min)	$C_2^=$ (bar)	$C_3^=$ (bar)	H_2 (bar)	N_2 (bar)
1	40	2	–	9.5	0.5	1.1	no 2nd prepolymerization					
2	40	2	1.0	8.5	0.5	1.1	no 2nd prepolymerization					
3	40	2	–	9.5	0.5	1.1	40	2	1.0	8.5	0.5	1.1

main polymerization of propylene shows high activity. However, when the catalyst is prepolymerized for 2 min in propylene, subsequently, in a coprepolymerization of ethylene and propylene, activity in the main polymerization has a normal value. In a main copolymerization after a propylene prepolymerization, reaction rate increases in the course of about 4 min to the doubled value.

Discussion: Optical Observations

The possibilities of the present method are diverse, but, in all the applications, it is clear that the direct comparison between different particles, with different properties, for example, particle size, in the same experiments under the same conditions, with the same history, is a big advantage of the method. It is no longer necessary to use average values for all the particles present in the experiment, but individual behavior of the particle can be studied.

Experimental method

It is clear from the results that the interval of values of the observed (or rather, calculated) reaction rates is relatively broad, and, to obtain solid information on polymerization kinetics, it is necessary to repeat the tests several times to reduce errors. As said, this is mainly due to the errors that occur in the determination of the 2-D surface. These errors are enlarged because of the 2-D—3-D translation. Another method for measuring single particle kinetics is the use of a thermobalance, as used by Garmatter (1999). This method does not have these problems and would be more suitable for the determination of single particle kinetics.

Microreactor as a tool for catalyst screening

In the development of new catalysts a number of different performance bench-scales can be distinguished. The microreactor presented here can be very useful in the determination of those performances.

Activity in Polymerization. This is probably the most obvious issue. A catalyst should show enough activity in polymerization at the desired process conditions. Although "conventional" lab-scale batch reactors (Meier et al., 2001a,b) are possibly more suited for a determination of kinetic behavior of a catalyst in gas-phase polymerization, the present method can be used to determine the kinetics of the individual particles, to be able to relate that to properties of those individual particles like initial particle size. Next to that, different catalyst systems, for example, catalyst activated in a different way, can directly be compared in the same polymerization test.

Induction Period. Besides the activity, one should know if the catalyst is showing an induction period. When it is, this can have negative effects on the application of the catalyst in existing technologies, for example, quick blowout of catalyst particles that are too small in a fluidized-bed reactor. However, on the other hand, it can also have positive effects like the prevention of thermal runaway, inherent in the largest catalyst particles in the initial stage of the polymerization without the application of a prepolymerization step. Although, in conventional kinetic reactors this induction behavior can be observed, it is not possible to compare the individual particles, and to relate the startup behavior of a particle to its (initial) properties. With the method presented here, this is possible.

Replication of Particle Shape. To obtain a final product with predictable powder morphology (powder morphology is a very important parameter of a product, as it determines flowability in the process equipment, but, for example, in the production of high-impact PP, the distribution of the rubbery phase over the homopolymer matrix depends on the particle morphology), it is vital that the shape of the catalyst particle is replicated in the growth of the polymer particle. With this method, we can compare not only the starting and final material, but also we can study the development of particle shape throughout the entire reaction.

Distribution of Active Material. To learn about the distribution of the active metal in the catalyst, one could analyze crosscuts of the particles using an EDX-type of analyses. However, one cannot be sure that all potential active metal present will really be activated. In the screening of the catalyst it is, therefore, important to make a comparison between the different catalyst particles to check if they behave in the same way. As said, the present method allows a direct comparison between different individual particles.

Currently Used Catalyst. From information shown here on shape replication and particle-size influence on single particle kinetics, we can conclude directly that the active sites in this catalyst are homogeneously distributed over the different catalyst particles. All particles start to grow at the same moment, immediately after the introduction of a monomer to the system, all particles replicate the initial shape of the catalyst particle, and the polymerization rate expressed per volume of catalyst does not depend on the initial particle size.

Comparing Gas-Phase Polymerization with Bulk Polymerization. When comparing the results of experiments carried out in this system to other experimental work with the same catalyst in the bulk polymerization of propylene (Pater et al., 2003), one has to keep in mind that catalyst preparation often differs significantly.

The results of the recipe variations demonstrate the activation of this catalyst to be a very fast process. When accepting that Ti^{2+} is not active in propylene polymerization (as commonly accepted in literature), it can be concluded that deactivation of the catalyst by overreduction of the titanium due to excessive concentrations of the aluminum alkyl does not occur at the levels used here, even at extremely long contact times. From the tests with a varied activation procedure, we can conclude that, during the interpretation of experimental results in the present work, the activation step does not need to be taken into account.

As stated, the same catalyst was also used in the liquid pool (bulk) polymerization of propylene. In principle, when the difference in monomer concentration is taken into account, the reaction rates observed in microreactor gas-phase polymerization should show the same values as liquid pool polymerization with the same catalyst. When assuming a first-order dependency of the reaction rate in monomer concentration, the reaction rates of the experiments can be compared. This first-order dependence is generally assumed in propylene polymerization with Ziegler-Natta catalysts (for example, Albizatti et al., 1996; Samson et al., 1999; Weickert et al., 1999).

Table 4. Comparison of Monomer Concentration and Reaction Rate in Liquid Pool and Microreactor Polymerization of Propylene

Temperature	(K)	313	323	333	343
Rho PPY	(mol/L)	11.31	10.81	10.26	9.59
Chi		0.833	0.760	0.692	0.629
Phi 1		0.440	0.514	0.600	0.702
Phi 2		0.118	0.095	0.079	0.066
$C_{m,LP}$	(mol/L)	4.972	5.553	6.159	6.733
$C_{m,9\,\mathrm{bar}}$	(mol/L)	1.336	1.026	0.806	0.636
$R_{p,LP}$	(kg/g·h)	5	13	26	55
$R_{p,\mathrm{Micro}}$	(kg/g·h)	0.27	0.35	0.47	0.72
$R_{p,LP}/C_{m,\mathrm{liq}}$	(kg·l/g_{cat}·h·mol)	1.006	2.341	4.222	8.168
$R_{p,\mathrm{micro}}/C_{m,\mathrm{gas}}$	(kg·l/g_{cat}·h·mol)	0.202	0.341	0.583	1.132
Ratio		5.0	6.9	7.2	7.2

Meier et al. (2001a) proposed a method to calculate monomer concentration at the active site, in the amorphous part of the polymer using the Flory-Huggins equation

$$\ln\left(\frac{P}{P^0}\right) = \ln(\phi) + (1-\phi) + \chi(1-\phi)^2 \qquad (2)$$

Table 4 shows the values for the interaction parameters, as reported by Meier et al. The concentration of monomer in the amorphous part of the polymer is calculated using these values and the density of the liquid monomer. When assuming a first-order dependency of the reaction rate in monomer concentration, the reaction rates in gas phase and in bulk can directly be compared. Figure 6 shows the temperature-dependent reaction rates for both cases (bulk and gas phase) corrected for the monomer concentration at the active site. It is shown that reaction rates in the microreactor are a factor 5–7 smaller than expected from liquid pool polymerization, despite the correction for the monomer concentration. The fact that temperature dependency is in both cases well described with Arrhenius, and yielding in very comparable activation energies, one could conclude that this "correction" is not giving the problem of the differences.

An important explanation for this difference can be found in the different preparation of the catalyst system. We concluded earlier that the activation has shown to be a fast process that is not very sensitive to TEA concentrations and contact time. However, in addition to the difference in the preparation of the catalyst, the concentrations of donor and cocatalyst during polymerization are different. In liquid pool conditions, D-donor and cocatalyst are injected into the liquid monomer and are available for the catalyst during the entire experiment. In microreactor experiments, the catalyst is activated, washed and dried, probably resulting in lower donor and cocatalyst concentrations on the catalyst surface with respect to liquid pool conditions. The difference in activity can, in our opinion, be ascribed to the difference in cocatalyst and donor concentration during the polymerization reaction.

Table 5. Typical Emissivity Factors for Components Present in the Microreactor System during Propylene Polymerization

Material	Size (micron)	Emissivity
Polypropylene particles, rough surface structure	500	0.69
Polypropylene particles, smooth surface structure	500	0.87
Polypropylene particles produced in microreactor	200	0.77
Ethylene-Propylene-Rubber particles from microreactor	200	0.79
Ziegler-Natta catalyst, activated	25	0.79

Effect of Ethylene Addition. From the pre- and copolymerization experiments, it seems as if the first monomer that the catalyst "sees" is important in the development of the system. Even after only a short prepolymerization in the presence of ethylene (experiment 12 in Table 2), the reaction rate of the homopropylene polymerization is permanently increased. We can think of different explanations for this effect.

It is possible that, just like hydrogen, the ethylene has the ability to activate certain catalyst sites. The presence of ethylene would increase the number of active sites, with that as the activity. When the catalyst is prepolymerized with propylene, the ethylene is not able to reach the potentially active sites because of hindrance by the polymer.

Another explanation would be different concentrations of monomer at the active sites of the catalyst, resulting in different reaction rates. In a copolymerization, a highly amorphous product is produced. One could imagine that solubility and diffusivity of monomers in this polymer is different from that in the homopolymer.

A third option would be that, at the active site, the ethylene would take part in activation of the titanium. An active site that has the presence of the ethylene molecule in the complex shows a larger ability to propagate the polymerization of propylene.

The enhancement of the propylene polymerization rate by the presence of ethylene is described in previous literature. To learn about the exact mechanisms playing a role in this effect, it would be necessary to perform a series of experiments with systematically varied types of comonomer to vary the rate of incorporation of both the monomers at its possible function in the complexation at the active site.

Results: Infrared Measurements

Particle temperature during polymerization

When beginning the observation of surface temperatures of reacting particles, it is important to realize that the measured surface temperature is the maximum temperature in the particle. It is pointed out often in literature (for example, Floyd et al., 1986a,b, 1987) that heat-transfer problems—large temperature rises in and around the particle—can be important in gas-phase reactions, especially at high activities and small catalyst particles. However, at the present low reaction rates—at a maximum of 2 $kg_{polymer}/g_{cat}$*h, compared to normal gas-phase polymerization reaction rates up to 10 $kg_{polymer}/g_{cat}$*h—temperature gradients will not exist inside the particle, possibly only at the very initial stage of the polymerization. (In the present case, however, a temperature gradient might occur, due to nonsymmetric heat removal from the particle by the underlying glass disk. This gradient will be small due to the relatively high heat conductivity of the polymer material.) The temperature observed on the top of the particle will be close to the maximum temperature in the particle.

Calibration. Infrared radiation detected by the infrared camera can be used to determine the surface temperature of

the objects in the observed area. The amount of infrared radiation coming from the objects is not only determined by the surface temperature of the object, but also by surface orientation and nature of the material, as indicated by Eq. 1

$$Q_{\text{rad}} = \sigma F_{\epsilon} F_a A\left(T_1^4 - T_2^4\right) \tag{1}$$

Figure 7 shows an infrared image of a coin that is well thermostated. Although one can be sure that temperature gradients in the material are negligible, the infrared image shows us differences of 20°C. The influence of the orientation of the surface complicates the interpretation of the image. The product of the material factor F_{ϵ} and the surface orientation factor F_a is called the emissivity factor ϵ. The σ in this equation is the Stefan-Boltzmann constant. Typically, infrared cameras use one emissivity factor for the interpretation of the complete observed area.

To be able to measure real particle temperatures, the emissivity of the materials used and the background radiation in the present setup were determined. First, deactivated particles were placed on electrical tape and stuck to a heated plate. The emissivity of the particles was determined outside the polymerization cell. Once these emissivity values were known, particles were placed in the reactor and the background temperature for the system was determined. The results of the calibration activities are shown in Table 5.

In the experiments, an emissivity factor of 0.77 is used for interpretation of the infrared data, as the calibration experiments showed that this is the most common value for the powders. The maximum theoretical uncertainty of the temperature measurements executed at 70°C is ± 4.9°C. Experiments and calibration tests show that a realistic estimation of the error made with the system is ± 1.0°C.

No Chemical Reaction. To be able to interpret results from polymerization experiments, tests were done using deactivated catalyst particles and deactivated polymer particles in the course of a typical experimental procedure. Figure 8 shows the observed temperature of 5 deactivated catalyst particles. It is interesting to see that, directly after injection of monomer, the surface temperature of the particles seems to increase with about 0.8°C. There are two possible explanations for this. When the temperature of the gases introduced into the system is slightly higher than the reactor temperature, this reactor temperature will increase when injecting the gas. Besides that, compression of the gas in the reactor, from 1 to, for example, 10 bar will increase gas temperature caused by the well-known Joule-Thomson effect. For propylene, the adiabatic temperature rise for propylene from 1 to 10 bar would be about 7°C. Of course, the system used here is far from adiabatic for the incoming gas. With the interpretation of the measured temperatures in the presence of chemical reaction, one should keep this effect in mind.

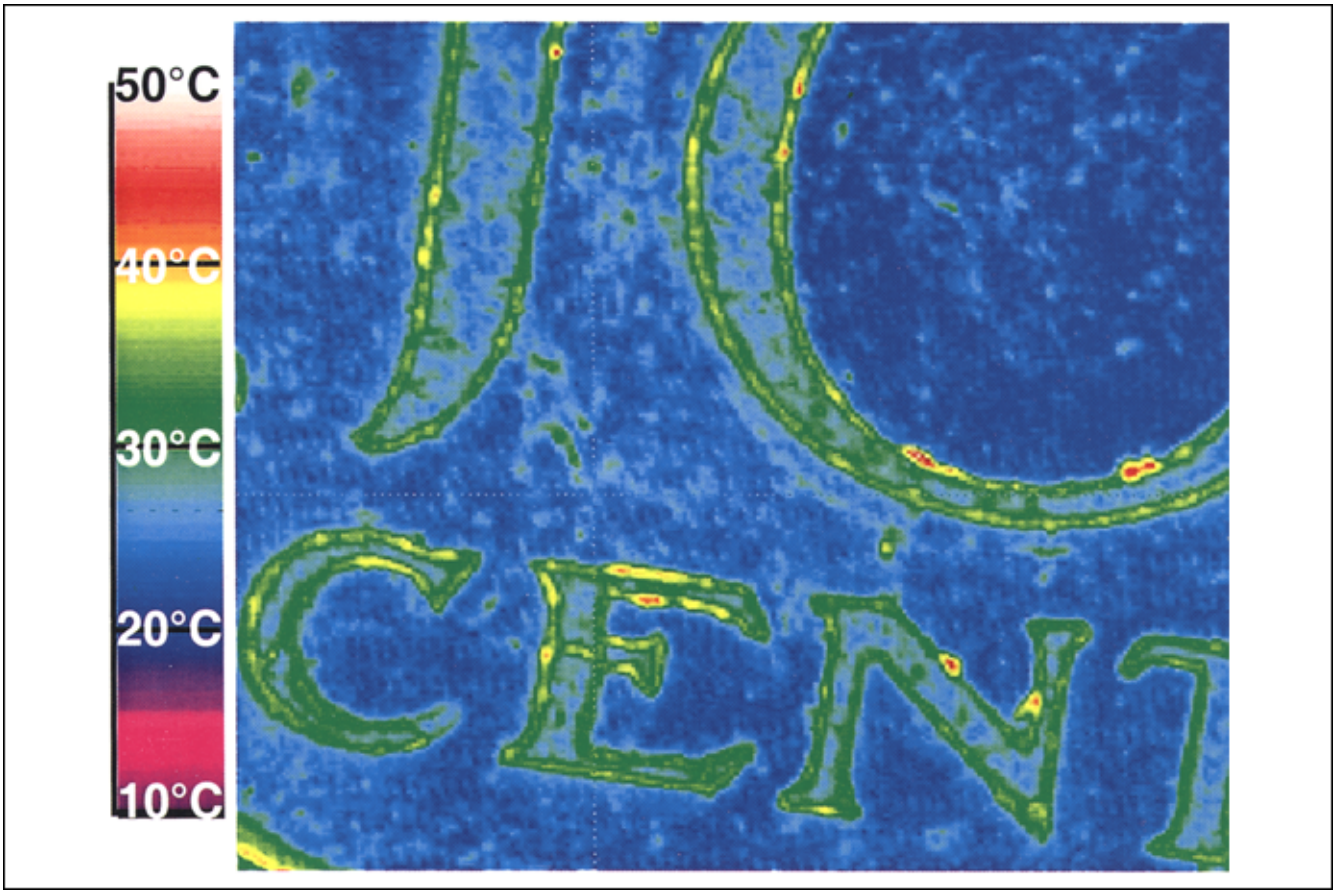

Figure 7. Infrared image of a well thermostated coin at about 25°C.

Difference in emissivity of different places on the coin becomes clear from the large apparent temperature differences.

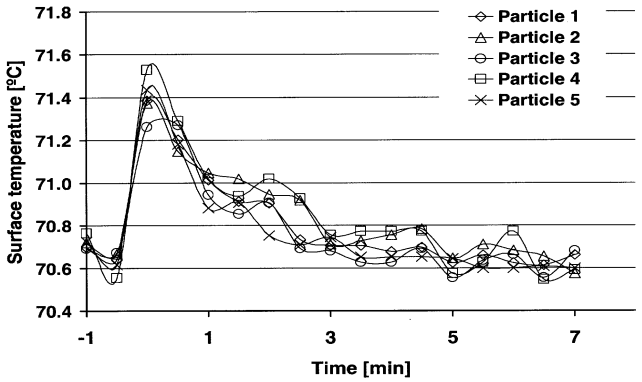

Figure 8. Observed surface temperatures of 5 individual deactivated particles.

Increase in temperature is caused by the introduction of monomer gas to the polymerization cell.

Homopolymerization of Propylene. The technique as described before, using the infrared imaging camera, was applied in the homopolymerization of propylene, indicated as experiment 16 in Table 2. The reaction rate of this polymerization was around 1.15 kg/g*h. The temperature profiles of different particles in that same experiment, presented in Figure 9, show a uniform behavior. The measurement uses the same value for the emissivity for the complete picture, with the value being obtained in calibration tests. This means that only the temperature value obtained from the center of the 2-D representation of the polymer can be trusted, as will be discussed in the section Discussion: Infrared Observations.

In the homopolymerization, starting at a temperature around 66°C, the temperature climbs to a maximum of 74°C on the surface of the particles, as measured in the center of the circular 2-D representation of the particle. The maximum is reached 7 min after the start of the polymerization. In the next 10 min the temperature falls to the reactor temperature, due to the increase of the heat-exchanging surface of the particle. Most particles reach the initial temperature again after about 16 min.

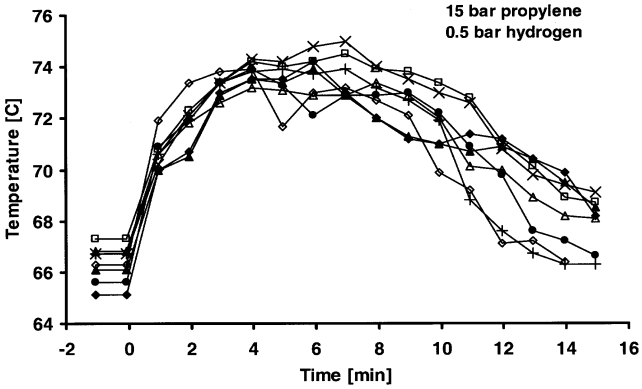

Figure 9. Observed surface temperatures of six individual particles in the same experiment (homopolymerization of propylene).

Copolymerization of Ethylene and Propylene. Figure 10 shows the surface temperature over time for different particles in the same copolymerization experiment of propylene and ethylene. As can be seen, the maximum temperatures are significantly higher than in the homopolymerization of propylene, due to the higher reaction rates. The maximum temperature is reached after 3 min and reaches a value of 83°C. After this maximum, the temperature decreases within 10–15 min to values close to the initial temperature. From optical measurements, we know that the decrease in temperature is not due to a decrease in reaction rate, as deactivation is small in these experiments. The decrease in particle temperature is, therefore, ascribed to the increasing heat removal, rather than the decreasing heat production.

Influence of Initial Particle Size on Particle Temperature. The method shown here allows us to make a direct comparison between different particles within the same polymerization experiments. It is not necessary to use the average value of all the particles within the experiment; one can directly observe individual temperatures. In this experiment, we recorded temperatures of smaller and larger particles within the same experiment. Figure 11 shows the temperature of the different particles over time in the copolymerization of ethylene and propylene. As expected, larger particles having a larger volume-to-surface ratio show larger temperature rises than the smaller particles. The power becomes clear of the method proposed here, that is, the ability to compare individual catalyst particles in exactly the same conditions without having to worry about experimental reproducibility.

Discussion: Infrared Observations

Observation method

It has been shown to be possible to observe with the hardware presented here growing polymer particles with an infrared camera and to measure its temperature this way. The resolution of the camera used is not optimal, but, to our knowledge, it is the best possibility available at this moment, for an acceptable price.

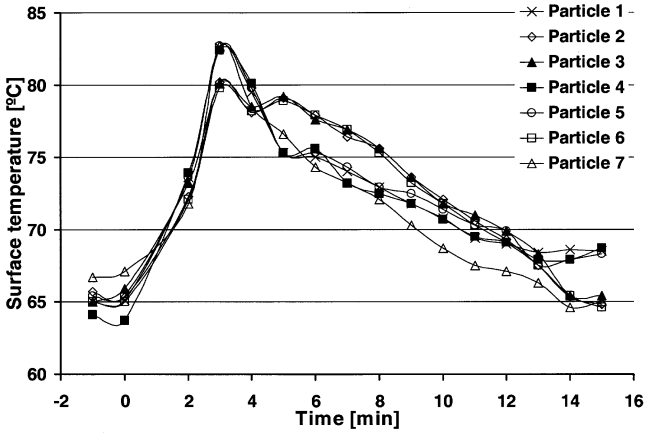

Figure 10. Surface temperature in time of seven different particles in the same copolymerization experiment.

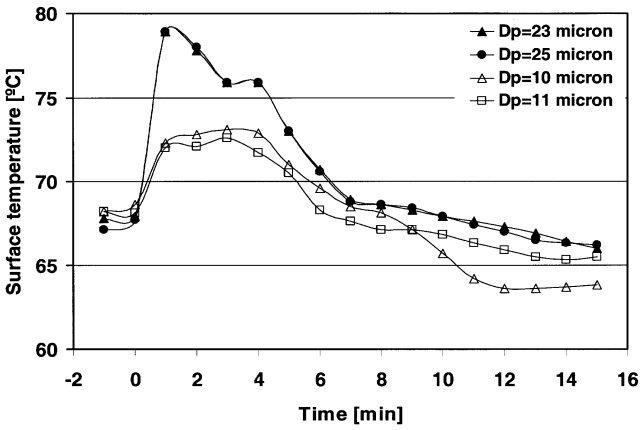

Figure 11. Influence of initial particle size on the particle's surface temperature over time, in the copolymerization of propylene with ethylene.

Larger particles show significant more overheating than the smaller ones, especially in the initial stage.

Another disadvantage of the proposed method is the underlying surface. Because of significant contact with the underlying glass, it is hard to draw conclusions on particle temperature for free particles. A complication of this matter is that particles are laying in a stagnant gas. Convective cooling, at Nusselt numbers larger than the theoretical value of 2 for the present situation, will change the particle's heat balance. Applying a moving gas in the polymerization cell would improve this situation.

At some points, the temperatures that were measured in the polymerization experiments do not agree with the expectations obtained from classical single particle models. The maximum temperature is reached after much more time than predicted. One of the reasons for this, we believe, is the underlying material that heats during polymerization. To quantify this influence, a simple calculation was made as follows.

Curved surfaces

With interpretation of the results, we have to keep in mind that the observed surfaces of the particles are curved. In Figure 12 it can be seen that an apparent temperature gradient exists over the particle. This effect is the same as mentioned before in the subsection Calibration, demonstrated in Figure 7. Both the coin in Figure 7 and the particle in the images of Figure 12 are free of significant temperature gradients. This means that, in the case of the existence of a real temperature gradient, it is hard to measure it with the methodology used here. In the results shown in the present work, the center of the 2-D representation is used to measure the temperature of the surface of the particle. This is also the position that was used for the determination of the emissivity values of the polymer particles.

Relation between reaction rate and temperature rise

It is possible to correlate between particle temperature increase and the reaction rate for the present polymerization cell. The reaction rate was varied by changing gas-phase composition: homopolymerization vs. copolymerization. With changes in the composition of the gas, also the heat exchanging properties of the gas were changed. Table 6 shows the temperature rise at three different reaction rates. It is clear that the temperature rise increases with the reaction rate.

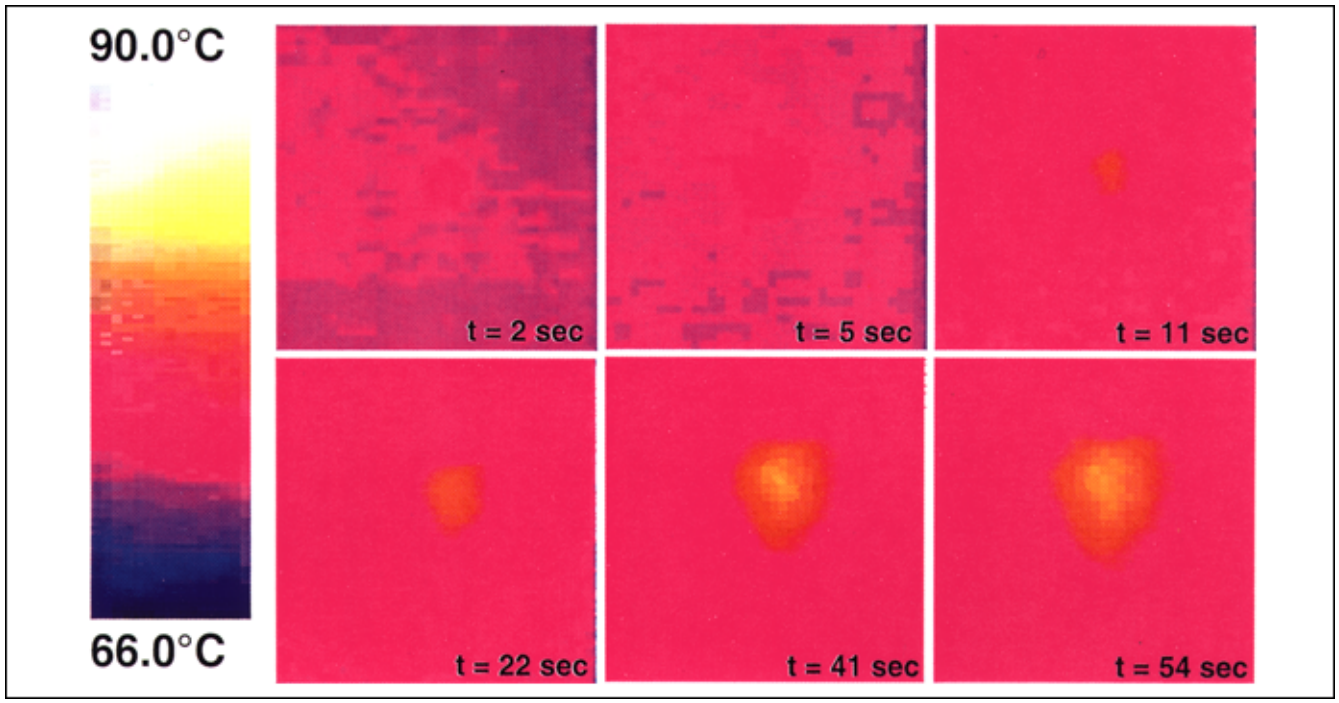

Figure 12. Infrared images of a growing particle in polymerization experiment, all with emissivity factor of $\epsilon = 0.77$.

To improve this correlation, one could modify the current polymerization cell in such a way that optical and infrared observations are allowed at the same moment. This facilitates at the same moment determination of single particle kinetic behavior and determination of the single particle temperature at the same particle.

Modeling of particle temperature

The rate of increase of the particle temperature, and the moment in time of the maximum value for the temperature, is different from predictions from single particle modeling work done before, for example, by Floyd et al. (1986a,b). The most probable explanation for this unexpected shift in time of the maximum particle temperature is the heating of the underlying surface. McKenna et al. (1999) showed in their CFD-work the importance of the direct solid-solid contact in the heat transfer of the polymer particle in a fluid-bed situation, especially for the smallest particles.

A simple model was worked out to investigate in a qualitative way the effect of heating of the underlying surface by the growing polymer particles. In this calculation, it was assumed that about 100 particles are present on the surface in this experiment. Some very rigorous assumptions were:

- No temperature gradients within the particle, nor within the gas phase or in the glass plate.
- Heat transfer between particle and surrounding can be described as heat transfer of a sphere in stationary gas phase ($Nu = 2$).
- All particles are perfectly spherical, have the same size, and are not agglomerated.
- Particle growth consists completely of polymer (no swelling, no change in particle porosity).
- A quasi steady state is assumed: $dRp/dt = 0$; $dCp/dT = 0$; $d\rho/dT = 0$.
- The convective contribution to heat transfer is neglected.

Table 6. Temperature Rises of Polymerizing Particles Dependent on the Polymerization Rate

Reaction Conditions						
$T_{reaction}$ (°C)	$C_3^=$ (bar)	$C_2^=$ (bar)	N_2 (bar)	H_2 (bar)	Reaction Rate ($kg_{polymer}/g_{cat}\cdot h$)	Temp. Rise (K)
					0.8	2
66	15	0	0	0.5	1.2	8
65	14	1	0	0.5	3	15–20

- Constant reaction rate and gas phase temperature are assumed.

Mass and Heat Balances. The following equation is used to describe the mass balance of the growing particle

$$\left(1-\epsilon_p\right)\frac{d\left(\rho_p V_p\right)}{dt} = R_p(t)M_m \tag{3}$$

with $R_p M_m$ being the reaction rate in kg/s.

Equation 4 is a representation of the heat balance of the polymer particle, with heat accumulation in the lefthand side term, and production, transfer to the gas, and transfer to the glass disk, respectively, in the righthand side term

$$\left(1-\epsilon_p\right)\frac{d\left(T_p\rho_p Cp_p V_p\right)}{dt} = -R\Delta H_r + A_{pg}(t)U_{pg}(t)\left[T_p(t)-T_g\right] + A_{dp}(t) \tag{4}$$

The values for the different parameters as used in the calculation are shown in Table 7.

Density and Heat Capacity of the Particle. The values for heat capacity and density of the particle are taken as fractionally weighed average values of the values for the pure

Table 7. Parameters used in Calculation of Particle Temperature

Variable	Description	Value	Dimension
$r_{particle}$	Radius particle	12.5	micron
r_{disk}	Radius disk	0.009	m
y_{disk}	Thickness disk	2	mm
ϵ	Particle porosity	0.4	-
$\rho_{catalyst}$	Density catalyst	2,300	$kg\cdot m^{-3}$
ρ_{PP}	Density polypropylene	900	$kg\cdot m^{-3}$
ρ_{disk}	Density disk	2,500	$kg\cdot m^{-3}$
ρ_{PPY}(gas, 10 bar, 70°C)	Density propylene	16.37	$kg\cdot m^{-3}$
ΔH_r	Heat of polymerization	104,000	$J\cdot mol^{-1}$
$C_{p,PP}$	Specific heat polypropylene	2,250	$J\cdot kg^{-1}\cdot K^{-1}$
$C_{p,cat}$	Specific heat catalyst	803	$J\cdot kg^{-1}\cdot K^{-1}$
$C_{p,PPY}$(gas, 10 bar, 70°C)	Specific heat propylene	1,667	$J\cdot kg^{-1}\cdot K^{-1}$
$C_{p,disk}$	Specific heat disk	800	$J\cdot kg^{-1}\cdot K^{-1}$
λ_{gas}	Heat conductivity propylene gas	1.7×10^{-2}	$W\cdot m^{-1}\cdot K^{-1}$
λ_{PP}	Heat conductivity polypropylene	0.12	$W\cdot m^{-1}\cdot K^{-1}$
λ_{disk}	Heat conductivity disk	9.3×10^{-1}	$W\cdot m^{-1}\cdot K^{-1}$
M_{PPY}	Mole weight propylene	0.042	$kg\cdot mol^{-1}$
R_p	Rate of polymerization	1	$kg_{PP}\cdot g_{cat}^{-1}\cdot h^{-1}$
$V_{reactor}$	Reactor volume	6	mL
n		1,000	-
x		1	micron
Nu	Nusselt number	2	-
$T(0)$	Initial temperature	340	K
Tg	Gas temperature	343	K

components. Of course, this is only of interest in the initial stage of the calculation, as the fraction of polymer quickly tends to one.

Heat-Transfer Coefficient from Particle to Gas. The heat-transfer coefficient for the particle in the gas mixture can be described with the well-known relation for the Nusselt number

$$Nu = \frac{U_{pg}(t)d_p(t)}{\lambda_g} \tag{5}$$

Nu can be estimated here with the empirical relation to the Reynolds and Prandl number

$$Nu = A + B(Re^a Pr^b) \tag{6}$$

where various values for the constants A, B, a, and b are mentioned in the literature, with A always being 2. The use of this relation for a particle of the size of some tens of microns is questionable, as also indicated in literature (McKenna et al., 1995). When using this relation and assuming a stagnant gas in the reactor, Nusselt becomes equal to 2.

Heat-Transfer Coefficient from Particle to Disk. To define a contact area between the underlying surface and the particle, which theoretically would be infinitely small in the case of a perfect spherical particle, all surface where the distance between particle and underlying material is smaller than the x micron is considered as being the contact area. This leads to the following definition of the contact area

$$A_{dp} = \pi \left| r^2 - (r - x)^2 \right| \tag{7}$$

The heat-transfer coefficient for the particle to the disk can be described as

$$Q = \left(\frac{\lambda}{L}\right) A_{dp}(T_p - T_d) \tag{8}$$

Of course, the A_{dp} is a somewhat difficult aspect here, as its value is not known, and adaptation of this value can significantly influence the results of the calculation.

This means

$$U_{dp} = \frac{\lambda_d}{L} \tag{9}$$

As the value for L is a variable, L will be set equal to its average value being the radius of the particle.

Figure 13 shows the result of calculation of the particle temperature as a function of time, when heat transfer from particle to gas and glass are both taken into account. One can see that the particle temperature is predicted to rise during the initial phase of the reaction until the maximum is reached, in this case after about 5 min, and to decrease after that. Calculations show that the predicted particle temperature is very sensitive in the number of particles that are put on the reactor plate, as this determines the heating up of the glass plate. Next to that, the temperature of the gas phase is very important, as this determines the heat transfer through the gas contact. This gas-phase temperature is changing in time and is not directly controlled. Therefore, it is difficult to exactly predict the heat transfer to the gas phase.

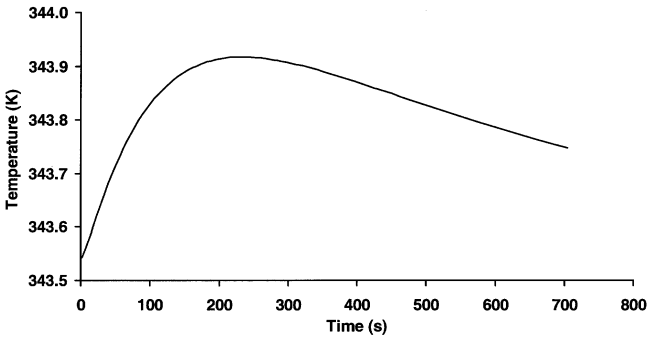

Figure 13. Result of calculation of particle temperature as function of time, with taking transfer to gas and to underlying surface into account.

Conclusions

Optical and infrared application

Although stirred bed reactors might be better suited for measurements of polymerization kinetics than the present system, a huge advantage of the present system is the ability to link kinetic information of individual particles to properties of these particles, rather than being obliged to settle for average values for all particles. Measurements in the system were shown to have good reproducibility between different particles in the same experiment, but a comparison between different experiments was poorer. Reaction rate curves showed some scatter due to blooming and background blurring. The method has been shown to be a good tool for catalyst screening, as it is possible to directly compare different catalyst particles and different catalyst systems in the same experiment, even relating results to particle properties like initial size.

The current setup is, as mentioned, still showing some drawbacks. First, the gas in the system is stagnant. To allow a more direct comparison between particles in the present system and particles in a fluidized-bed system, a convective flow should be present in the system. In addition, the contact between the particle and the underlying surface significantly influence the particle's heat balance. The heat exchange between the particle and the underlying surface should be significantly minimized (either through reducing the contact area or through reducing the heat exchange coefficient). To summarize the strong points of the method:

- The method allows direct measurement of particle surface temperature (never done before);
- It allows comparison of individual particles with respect to: polymerization kinetics (induction period, rate of polymerization deactivation); shape replication and powder morphology development; and particle temperature during polymerization.
- It allows a comparison of different catalysts in the same polymerization run; and

• The method is quick (5 polymerization tests in an 9 h working day).

Current catalyst system

The currently used catalyst showed a very good shape replication and did not show any significant induction period. Activation energy of the system was about 52 kJ/mole. The concentrations of donor and cocatalyst during either the activation step or the activation time did not change its activity in polymerization.

When comparing the activity of the catalyst system in the gas phase to the polymerization rate in liquid propylene, a decrease of a factor of 5 was found. This is ascribed to the absence of a cocatalyst and an electron donor during polymerization in gas phase, which is carried out in the microreactor.

A short prepolymerization in the presence of some ethylene (as a copolymerization) showed a remarkable and persistent effect of increasing the reaction rate in the main homopolymerization of the catalyst. A more systematic view of copolymerization and accelerating effects of comonomers is necessary to explain this.

The infrared observations have shown that it is possible to measure particle temperature during polymerization. Observed temperature rises were strongly correlated, as expected, with catalyst particle size and polymerization rate. With the catalyst used here, the temperature rise was up to 20 deg at a reaction rate of about 3 $kg_{polymer}/g_{cat} \cdot h$ at 70°C. The temperature-time profiles measured on the current system did not agree with expectations from single particle models. The main reason mentioned to explain this discrepancy is the presence of the underlying surface of the particle. Temperatures are not constant in this glass plate, resulting in a drift in the heat exchange between the particle and its surroundings. A simple model was used to qualitatively describe this effect.

Acknowledgments

The work presented in this article was carried out in cooperation with The Dow Chemical Company, Freeport, TX. The authors wish to thank Dow for both the financial and the intellectual input. The aluminum alkyls used in the work were kindly donated by AkzoNobel. The technical assistance of Gert Banis, Fred ter Borg, Karst van Bree, and Geert Monnink is greatly appreciated.

Literature Cited

Albizatti, E., U. Giannini, G. Collina, L. Noristi, and L. Resconi, *Polypropylene Handbook*, E. G. Moore, ed., Carl Hanser Verlag, Munich, Vienna, New York (1996).

Annamalai, J., C. Ballandis, M. Somani, M. A. Liauw, and D. Luss, "Effects of Reactant Composition and Non-uniformities on Temperature Fronts," *J. Chem. Phys.*, **107**, 1896 (1997).

Annamalai, J., M. A. Liauw, and D. Luss, "Temperature Patterns on a Hollow Cylindrical Catalytic Pallet," *Chaos*, **9**, 36 (1999).

Baker, R. T. K., P. S. Harris, and R. J. Waite, "Continuous Electron Microscopic Observation of the Behavior of Ziegler-Natta Catalysts," *Pol. Lett.*, **11**, 45 (1973).

Bartke, M., A. Wartmann, and K.-H. Reichert, "Gas Phase Polymerization of Butadiene. Data Acquisition using Minireactor Technology and Particle Modeling," *J. of Appl. Poly. Sci.*, **87**, 270 (2003).

Corradini, P., V. Busico, and G. Guerra, "Possible Models for the Steric Control in the Heterogeneous High-Yield and Homogeneous Ziegler-Natta Polymerizations of 1-alkenes," *Transition Metals and Organometallics as Catalysts for Olefin Polymerization*, W. Kaminsky and H. Sinn, eds., Springer-Verlag, Berlin, p. 337 (1988).

Eberstein, C., B. Garmatter, K.-H. Reichert, and G. Sylvester, "Gasphasenpolimerisation von Butadien," *Chemie Ingenieur Technik*, **68**, 820 (1996).

Floyd, S., K. Y. Choi, T. W. Taylor, and W. H. Ray, "Polymerization of Olefins Through Heterogeneous Catalysis: III. Polymer Particle Modeling—Analysis of Intraparticle Heat and Mass Transfer Effects," *J. Appl. Poly. Sci.*, **32**, 2935 (1986a).

Floyd, S., K. Y. Choi, T. W. Taylor, and W. H. Ray, "Polymerization of Olefins Through Heterogeneous Catalysis: IV. Modeling of Mass and Heat Transfer Resistance in the Polymer Particle Boundary Layer," *J. Appl. Poly. Sci.*, **31**, 2231 (1986b).

Floyd, S., T. Heiskanen, T. W. Taylor, G. E. Mann, and W. H. Ray, "Polymerization of Olefins Through Heterogeneous Catalysis: VI. Effect of Particle Heat and Mass Transfer on Polymerization Behavior and Polymer Properties," *J. Appl. Poly. Sci.*, **33**, 1021 (1987).

Galli, P., "Forty Years of Industrial Developments in the Field of Isotactic Polyolefins," *Macromol. Symp.*, **89**, 13 (1995).

Garmatter, B., "Anwendung der Mikrogravimetrie zur Erfassung kinetischer und stofftransportspezifischer Daten von Polymerisation aus der Gasphase," PhD Thesis, Technical University of Berlin (1999).

Holzwarth, A., H-W. Schmidt, and W. F. Maier, "Detection of Catalytic Activity in Combinatorial Libraries of Heterogeneous Catalysts by IR Thermography," *Angew. Chem. Int. Ed.*, **37**, 2644 (1998).

Kaneko, Y., "Particle Behavior and Reaction in Gas Phase Olefin Polymerization Reactors," PhD Thesis, Tokyo University of Agri. & Tech., Japan (2000).

Liauw, M. A., M. Somani, J. Annamalai, and D. Luss, "Oscillating Temperature Pulses During CO and Oxidation on a Pd/Al_2O_3 Ring," *AIChE J.*, **43**, 1519 (1997).

Lobban, L., G. Philippou, and D. Luss, "Standing Temperature Waves on Electrically Heated Catalytic Ribbons," *J. Phys. Chem.*, **93**, 733 (1989).

McKenna, T. F., J. Dupuy, and R. Spitz, "Modeling of Transfer Phenomena on Heterogeneous Ziegler Catalysts: Differences between Theory and Experiment in Olefin Polymerization (An Introduction)," *J. Appl. Poly. Sci.*, **57**, 371 (1995).

McKenna, T. F., R. Spitz, and D. Cokljat, "Heat Transfer from Catalyst with Computational Fluid Dynamics," *AIChE J.*, **45**, 2392 (1999).

Meier, G. B., G. Weickert, and W. P. M. van Swaaij, "Comparison of Gas and Liquid Phase Polymerization of Propylene with a Heterogeneous Metallocene Catalyst," *J. Appl. Poly. Sci.*, **81**, 1193 (2001a).

Meier, G. B., G. Weickert, and W. P. M. van Swaaij, "Gas-Phase Polymerization of Propylene: Reaction Kinetics and Molecular Weight Distribution," *J. Pol. Sci. Pol. Chem.*, **39**, 500 (2001b).

Moates, F. C., M. Somani, J. Annamalai, J. T. Richardson, D. Luss, and R. C. Willson, "Infrared Thermographic Screening of Combinatorial Libraries of Heterogeneous Catalysts," *Ind. Eng. Chem. Res.*, **35**, 4801 (1996).

Oleshko, V. P., P. A. Crozier, R. D. Cantrell, and A. D. Westwoord, "In-situ and Ex-Situ Microscopy Study of Gas Phase Propylene Polymerization over a High Activity $TiCl_4$-$MgCl_2$ Heterogeneous Ziegler-Natta Catalyst," *Macromol. Rapid Commun.*, **22**, 34 (2001).

Pater, J. T. M., P. Roos, G. Weickert, K. R. Westerterp, F. Shimizu, and G. Ko, "Integral Research Aspects of Gas Phase Olefin Polymerization: Kinetics, Absorption and Fluidization," *DECHEMA Monographs, 6th Int. Workshop on Polymer Reaction Engineering*, Berlin, **134**, 103 (Oct. 5–7, 1998).

Pater, J. T. M., G. Weickert, and W. P. M. van Swaaij, "New Method for Online Observation of Growing Polyolefin Particles," *Chimia*, **55**, 231 (2001).

Pater, J. T. M., G. Weickert, and W. P. M. van Swaaij, "Propene Bulk Polymerization Kinetics: Role of Prepolymerization and Hydrogen," *AIChE J.*, **49**, 180 (2003).

Pawlicki, P. C., and R. A. Schmitz, *Chem. Eng. Prog.*, **2**, 350 (1987).

Reetz, T. M., M. H. Becker, M. Liebl, and A. Fürstner, "IR-Thermographic Screening of Thermoneutral or Endothermic Transformations: The Ring-Closing Olefin Metathesis Reaction," *Angew. Chem. Int. Ed.*, **39**, 1236 (2000).

Reetz, T. M., M. H. Becker, H.-W. Klein, and D. Stöckigt, "A Method for High-Throughput Screening of Enantioselective Catalysts," *Angew. Chem. Int. Ed.*, **38**, 1758 (1998a).

Reetz, T. M., M. H. Becker, K. M. Kühling, and A. Holzwarth, "Time-Resolved IR-Thermographic Detection and Screening of

Enantioselectivity in Catalytic Reactions," *Angew. Chem. Int. Ed.*, **37**, 2647 (1998b).
Samson, J. J. C., P. J. Bosman, G. Weickert, and K. R. Westerterp, "Liquid-Phase Polymerization of Propylene with a Highly Active Ziegler-Natta Catalyst. Influence of Hydrogen, Cocatalyst, and Electron Donor on the Reaction Kinetics," *J. Pol. Sci.— Part A: Pol. Chem.*, **37**, 219 (1999).
Somani, M., M. A. Liauw, and D. Luss, "Evolution and Impact of Temperature Patterns during Hydrogen Oxidation on a Ni Ring," *Chem. Eng. Sci.*, **52**, 2331 (1997).
Weickert, G., G. B. Meier, J. T. M. Pater, and K. R. Westerterp, "The Particle as Microreactor: Catalytic Propylene Polymerizations with Supported Metallocenes and Ziegler-Natta Catalysts," *Chem. Eng. Sci.*, **54**, 3291 (1999).
Zoellner, K., and K.-H. Reichert, "Gas Phase Polymerization of Butadiene. Kinetics, Particle Size Distribution and Modeling," *Chem. Eng. Sci.*, **56**, 4099 (2001).

Manuscript received Sept. 19, 2001, and revision received Sept. 4, 2002.